

Analysis of Emission Shapes

Paweł Danielewicz^a

National Superconducting Cyclotron Laboratory and
Department of Physics and Astronomy, Michigan State University,
East Lansing, MI 48824, USA

Abstract. Shapes of relative emission sources can be accessed by expanding shapes of correlations at low relative velocities in pair center of mass in Cartesian harmonics. Coefficients of expansion for correlations are related to the respective coefficients of expansion for the sources through one dimensional integral transforms involving properties of pair relative wavefunctions. The methodology is illustrated with analyses of NA49 and PHENIX correlation data.

Keywords: interferometry, HBT, correlations, emission source, Cartesian harmonics

PACS: 25.70.Pq, 25.75.Gz

1. Introduction

Correlations of particles at low relative velocities have been used to determine sizes of emitting regions in heavy-ion reactions [1, 2]. In general, the smaller the emitting region the stronger are final-state effects in emission and stronger correlations between the emitted particles. However, shapes of emitting regions are also of interest. For example, a prolonged emission of particles, such as associated with a transitional behavior from quark-gluon plasma, can produce a relative emission source elongated in the direction of pair total momentum [3]. When the final-state effects are due to pure identity interference, the correlation function represents a Fourier-transform of the relative emission source [4]. Most commonly, in the past, source shapes have been analyzed for charged pions only, by representing the sources in terms of a single anisotropic Gaussian, allowing to interpret Coulomb-corrected correlation functions in terms of the Fourier-transformed Gaussian [1, 2]. Here, I discuss an alternative strategy, where the correlation function and source functions are expanded in surface spherical harmonics. Of the latter, the Cartesian harmonics [5] exhibit particularly pleasing properties for the purpose. The strategy is not confined to correlations dominated by identity interference.

2. Correlations at Low Relative Velocity

Possibility of learning on the geometry of emitting regions in reactions relies on the ability to factorize the amplitude for the reaction into a wavefunction $\Phi_{\mathbf{q}}^{(+)}$, for the pair of detected particles, and an amplitude remnant. At low relative velocity, $|\Phi_{\mathbf{q}}^{(+)}|^2$ may exhibit pronounced spatial features such as associated with identity interference, resonances or Coulomb repulsion. The wavefunction features can be regulated by changing the relative particle momentum \mathbf{q} . The amplitude remnant, squared within a cross section and summed over the unobserved particles and integrated over their momenta, yields S' which represents general features of reaction geometry, without a significant variation with \mathbf{q} . When examining the inclusive two-particle cross-section then, the structures in $|\Phi^{(+)}|^2$ can be used to explore the geometry in S' :

$$\frac{d\sigma}{d\mathbf{p}_1 d\mathbf{p}_2} = \int d\mathbf{r} S'_{\mathbf{P}}(\mathbf{r}) |\Phi_{\mathbf{q}}^{(-)}(\mathbf{r})|^2. \quad (1)$$

The naive expectation, met at large q for a multi-particle final state, is that the emission of two particles is uncorrelated. It is then interesting to normalize the two-particle cross section with a product of single-particle cross sections and to look for the evidence of correlations:

$$\mathcal{R}(\mathbf{q}) = \frac{\frac{1}{\sigma} \frac{d\sigma}{d\mathbf{p}_1 d\mathbf{p}_2}}{\frac{1}{\sigma} \frac{d\sigma}{d\mathbf{p}_1} \frac{1}{\sigma} \frac{d\sigma}{d\mathbf{p}_2}} - 1 = \int d\mathbf{r} \left(|\Phi_{\mathbf{q}}^{(-)}(\mathbf{r})|^2 - 1 \right) S_{\mathbf{P}}(\mathbf{r}). \quad (2)$$

The second equality follows from the fact that, at large q , the relative wavefunction squared is equal, on the average, to 1; in combining this with $\mathcal{R} \simeq 0$ at large q , the source S , following the cross-section normalization, turns out to be normalized to 1, $\int d\mathbf{r} S(\mathbf{r}) = 1$. Equation (2) links the correlation function \mathcal{R} to the interplay of deviations of the relative wavefunction from 1 with the geometry in S . Normalized to 1, S may be interpreted as the probability density for emitting the two particles at the relative separation \mathbf{r} within the particle center of mass. The emission is integrated over time, as far as S is concerned.

3. Correlations in Terms of Cartesian Harmonics

Given $\mathcal{R}(\mathbf{q})$ and $|\Phi|^2$, one can try to learn about S ; mathematically, this represents a difficult problem involving an inversion of the integral kernel $K(\mathbf{q}, \mathbf{r}) = |\Phi_{\mathbf{q}}^{(-)}(\mathbf{r})|^2 - 1$, in three dimensions. The situation gets simplified by the fact that K depends only on q , r and the angle $\theta_{\mathbf{q}\mathbf{r}}$. Correspondingly, the kernel can be expanded in Legendre polynomials:

$$K(\mathbf{q}, \mathbf{r}) = \sum_{\ell} (2\ell + 1) K_{\ell}(q, r) P^{\ell}(\cos \theta). \quad (3)$$

Upon expanding the correlation and source functions in spherical harmonics $Y^{\ell m}$, $\mathcal{R}(\mathbf{q}) = \sqrt{4\pi} \sum_{\ell m} \mathcal{R}^{\ell m}(q) Y^{\ell m}(\hat{\mathbf{q}})$, one finds that the three-dimensional relation (2) is equivalent to a set of one-dimensional relations for the corresponding harmonic coefficients [4],

$$\mathcal{R}^{\ell m}(q) = 4\pi \int dr r^2 K_{\ell}(q, r) S^{\ell m}(r). \quad (4)$$

For weak anisotropies, only low- ℓ coefficients of \mathcal{R} or S are expected to be significant. The $\ell = 0$ version of (4) connects the angle-averaged functions.

The above results suggest an analysis of the correlation functions and source functions in terms of the harmonic coefficients. An issue, however, is that it is cumbersome to analyze real functions in terms of complex coefficients that lack a clear interpretation for $\ell \geq 1$. It becomes then natural to seek another basis for the directional decomposition of correlation functions and sources, one that would be real and have a clear geometric meaning. Such a basis may be constructed starting from a unit direction vector $\hat{n}_{\alpha} = (\sin \theta \cos \phi, \sin \theta \sin \phi, \cos \theta)$. A convenient choice of axes relative to which the angles are determined in a reaction is z along the beam axis, x along the transverse component of pair total momentum and y perpendicular to the two other axes.

The tensor product of ℓ vectors \hat{n}_{α} yields a symmetric rank- ℓ Cartesian tensor that is a combination of spherical tensors of rank $\ell' \leq \ell$ and the same evenness as ℓ :

$$(\hat{n}^{\ell})_{\alpha_1 \dots \alpha_{\ell}} \equiv \hat{n}_{\alpha_1} \hat{n}_{\alpha_2} \dots \hat{n}_{\alpha_{\ell}} = \sum_{\ell' \leq \ell, m} c_{\ell' m} Y^{\ell' m}. \quad (5)$$

A projection operator \mathcal{P} may be constructed in the space of symmetric rank- ℓ tensors, out of a combination of Kronecker δ -symbols, that makes a symmetric tensor traceless,

$$\sum_{\alpha} (\mathcal{P} \hat{n}^{\ell})_{\alpha \alpha \alpha_3 \dots \alpha_{\ell}} = 0. \quad (6)$$

The tracelessness of $(\mathcal{P} \hat{n}^{\ell})$ ensures [5, 6] that the products $r^{\ell} (\mathcal{P} \hat{n}^{\ell})_{\alpha_1 \dots \alpha_{\ell}}$ are solutions of the Laplace equation and, thus, the $(\mathcal{P} \hat{n}^{\ell})_{\alpha_1 \dots \alpha_{\ell}} \equiv \mathcal{A}_{\alpha_1 \dots \alpha_{\ell}}^{(\ell)} \equiv \mathcal{A}_{x^{\ell_x} y^{\ell_y} z^{\ell_z}}^{(\ell)}$ are combinations of spherical harmonics of rank ℓ only. In the above, ℓ_x , ℓ_y and ℓ_z are the number of times of repeated, respectively, x , y and z indices in the symmetric tensor $\mathcal{P} \hat{n}^{\ell} \equiv \mathcal{A}^{(\ell)}$, $\ell_x + \ell_y + \ell_z = \ell$. The Cartesian tensor components of $\mathcal{A}^{(\ell)}$ are real and may be used to replace $Y^{\ell m}$. The lowest-rank tensors are:

$$\begin{aligned} \mathcal{A}^{(0)} &= 1, \quad \mathcal{A}_{\alpha}^{(1)} = \hat{n}_{\alpha}, \quad \mathcal{A}_{\alpha_1 \alpha_2}^{(2)} = \hat{n}_{\alpha_1} \hat{n}_{\alpha_2} - \frac{1}{3} \delta_{\alpha_1 \alpha_2}, \\ \mathcal{A}_{\alpha_1 \alpha_2 \alpha_3}^{(3)} &= \hat{n}_{\alpha_1} \hat{n}_{\alpha_2} \hat{n}_{\alpha_3} - \frac{1}{5} (\delta_{\alpha_1 \alpha_2} \hat{n}_{\alpha_3} + \delta_{\alpha_1 \alpha_3} \hat{n}_{\alpha_2} + \delta_{\alpha_2 \alpha_3} \hat{n}_{\alpha_1}). \end{aligned} \quad (7)$$

The completeness relation in terms of the Cartesian components is [6]

$$\begin{aligned}\delta(\Omega' - \Omega) &= \frac{1}{4\pi} \sum_{\ell} \frac{(2\ell+1)!!}{\ell!} \sum_{\alpha_1 \dots \alpha_{\ell}} \mathcal{A}_{\alpha_1 \dots \alpha_{\ell}}^{(\ell)} \mathcal{A}_{\alpha_1 \dots \alpha_{\ell}}^{(\ell)} \\ &= \frac{1}{4\pi} \sum_{\ell} \frac{(2\ell+1)!!}{\ell!} \sum_{\alpha_1 \dots \alpha_{\ell}} \mathcal{A}_{\alpha_1 \dots \alpha_{\ell}}^{(\ell)} \hat{n}_{\alpha_1} \dots \hat{n}_{\alpha_{\ell}},\end{aligned}\quad (8)$$

where the second equality follows from $\mathcal{D} = \mathcal{D}^{\top} = \mathcal{D}^2$. The completeness relation can be utilized for expanding \mathcal{R} or S in terms of the Cartesian tensor components

$$\mathcal{R}(\mathbf{q}) = \int d\Omega' \delta(\Omega' - \Omega) \mathcal{R}(\mathbf{q}') = \sum_{\ell} \sum_{\alpha_1 \dots \alpha_{\ell}} \mathcal{R}_{\alpha_1 \dots \alpha_{\ell}}^{(\ell)}(q) \hat{q}_{\alpha_1} \dots \hat{q}_{\alpha_{\ell}}, \quad (9)$$

where the coefficients are angular moments,

$$\mathcal{R}_{\alpha_1 \dots \alpha_{\ell}}^{(\ell)}(q) = \frac{(2\ell+1)!!}{\ell!} \int \frac{d\Omega_{\mathbf{q}}}{4\pi} \mathcal{R}(\mathbf{q}) \mathcal{A}_{\alpha_1 \dots \alpha_{\ell}}^{(\ell)}. \quad (10)$$

With (4) and with the \mathcal{R} and S Cartesian coefficients being identical combinations of the respective $Y^{\ell m}$ -coefficients, the corresponding \mathcal{R} and S Cartesian coefficients are directly related to each other,

$$\mathcal{R}_{\alpha_1 \dots \alpha_{\ell}}^{(\ell)}(q) = 4\pi \int dr r^2 K_{\ell}(q, r) \mathcal{S}_{\alpha_1 \dots \alpha_{\ell}}^{(\ell)}(r). \quad (11)$$

For weak anisotropies, only low- ℓ Cartesian coefficients for the source or correlation matter,

$$\mathcal{R}(\mathbf{q}) = \mathcal{R}^{(0)}(q) + \sum_{\alpha} \mathcal{R}_{\alpha}^{(1)}(q) \hat{q}_{\alpha} + \sum_{\alpha_1 \alpha_2} \mathcal{R}_{\alpha_1 \alpha_2}^{(2)}(q) \hat{q}_{\alpha_1} \hat{q}_{\alpha_2} + \dots \quad (12)$$

The correlation coefficients $\mathcal{R}^{(\ell)}$ allow to summarize three-dimensional information accumulated in the measurements, in terms of one-dimensional plots. With (9) and (12), the values of correlation (and similarly source) function in the $+z$ direction are given by

$$\mathcal{R}(q) = \mathcal{R}^{(0)}(q) + \mathcal{R}_z^{(1)}(q) + \mathcal{R}_{zz}^{(2)}(q) + \dots$$

and in the xz plane at 45° degrees by

$$\mathcal{R}(q) = \mathcal{R}^{(0)}(q) + \frac{1}{\sqrt{2}} \mathcal{R}_z^{(1)}(q) + \mathcal{R}_{xz}^{(2)}(q) + \frac{1}{2} \left(\mathcal{R}_{xx}^{(2)}(q) + \mathcal{R}_{zz}^{(2)}(q) \right) + \dots$$

The coefficients $\mathcal{R}^{(\ell)}$ can be found through angular integration (10) or by fitting the expansion series (12) to the dependence of data on spherical angle. The latter procedure can be particularly useful for an experiment blind in certain directions. For relating the correlation coefficients to source coefficients, the two-body problem

needs to be solved for the wavefunction $\Phi_{\mathbf{q}}^{(-)}(\mathbf{r})$. Not only identity interference, but also Coulomb and strong interactions give rise to structures in $|\Phi_{\mathbf{q}}^{(-)}(\mathbf{r})|^2$ that yield finite kernels K_ℓ for multipolarities $\ell > 0$ [6]. Contrary to naive expectations, even strong interactions acting in s -wave only produce finite kernels K_ℓ at $\ell > 0$. With regard to the Coulomb interactions, there is no good reason trying to correct for them [2], as they can provide access to source deformations just as the identity interference can. Features of the source can be accessed in (11) by assuming a parameterized shape of the source and fitting source parameters to the correlation coefficients, or by imaging source coefficients in the same manner as for $\ell = 0$ [7].

4. Sample Results from Data Analysis

The number of angular expansion coefficients that need to be considered for the correlation and source functions can be quite small. Thus, for pairs of identical particles, such as identical pions, the correlation functions are symmetric under inversion of relative momentum, $\mathbf{q} \rightarrow -\mathbf{q}$, meaning that only even- ℓ components are finite. Around midrapidity of a symmetric system, such as Pb + Pb or Au + Au, the correlation function should be symmetric with respect to the interchange of forward and backward directions, $q_z \rightarrow -q_z$, meaning that only even- z components of the functions can be finite. When the correlation functions are averaged over reaction-plane orientation, they are symmetric under interchange of the orientation of sideway axis, $q_y \rightarrow -q_y$, meaning that only even- y components of the functions can be finite. In the end, as a consequence of the above, the correlation function in the considered situation must be invariant under the interchange of the orientation of outward axis, $q_x \rightarrow -q_x$, meaning that only even- x components of the functions can be finite. For $\ell \leq 4$, the finite Cartesian moments are then $\ell = 0$, x^2 , y^2 and z^2 for $\ell = 2$ and x^4 , y^4 , z^4 , $x^2 y^2$, $x^2 z^2$ and $y^2 z^2$ for $\ell = 4$. Due to the tracelessness of the tensors from Cartesian components, however, only 2 of the above $\ell = 2$ components are independent and only 3 of the $\ell = 4$. Thus, depending on data statistics, the dependence of anisotropic correlation function on spherical angle at any q can be described with either 3, for $\ell \leq 4$, or 6, for $\ell \leq 6$, functions of relative momentum q .

Figure 1 shows $\ell = 0$ and $\ell = 2$ Cartesian harmonic results for the midrapidity $\pi^-\pi^-$ correlation functions measured by the NA49 Collaboration in central Pb + Pb collisions at $\sqrt{s} = 17.3$ A GeV. The $\ell = 0$ panels show the correlation function averaged over directions of relative momentum and the $\ell = 2$ panels illustrate the quadrupole deformation of the function. The z^2 coefficients are given by negative of the sum of x^2 and y^2 coefficients, $\mathcal{R}_{z^2}^{(2)} = -(\mathcal{R}_{x^2}^{(2)} + \mathcal{R}_{y^2}^{(2)})$. No Coulomb corrections have been applied to the data. On the other hand, effects of Coulomb interactions are accounted for directly in relating source functions to the data. In the left panels of Fig. 1, it is seen that a single Gaussian source fails to describe the data at low relative momenta. In the right panels, on the other hand, it is seen that a source combining two Gaussian sources provides a much better description of the data.

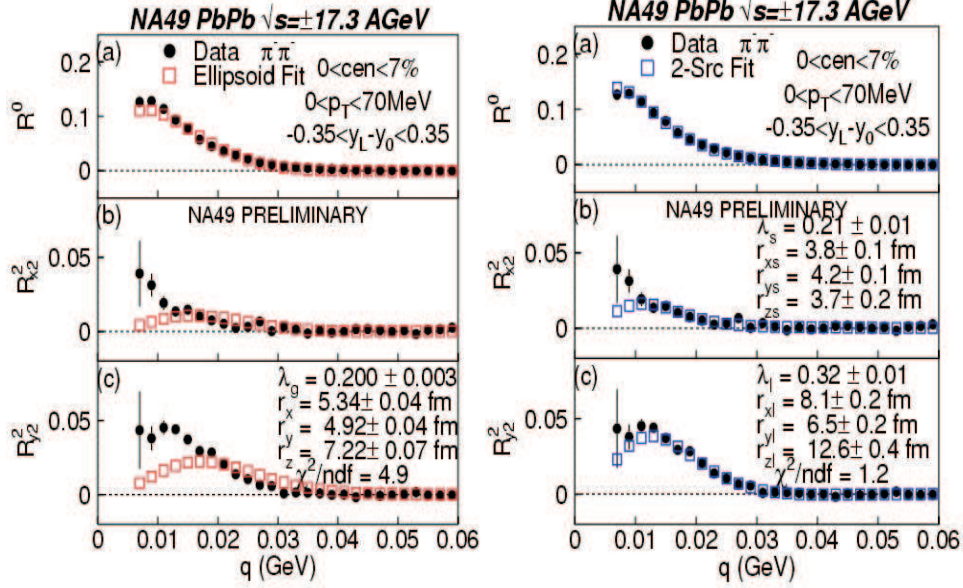


Fig. 1. $\ell = 0$ and two independent $\ell = 2$ angular moments of $\pi^+ - \pi^-$ correlation functions in central Pb + Pb collisions at $\sqrt{s} = 17.3$ A GeV. Filled circles represent measurements of the NA49 Collaboration [8]. Squares in the left panels represent a fit to the data with a source in the form of an anisotropic Gaussian. Squares in the right panels represent a fit to the data with a source combining two anisotropic Gaussians.

Figure 2 shows next source values along x , y and z axes, from summing $\ell = 0$ and $\ell = 2$ source coefficients deduced from the coefficients of correlation function measured in central Pb + Pb collisions at $\sqrt{s} = 8.9$ A GeV and $\sqrt{s} = 17.3$ A GeV [8]. Aside from the single and two Gaussian results, also source values obtained through imaging [7] are shown. The imaged sources usually yield a very good description of measured correlations. It is seen in the figure that the fitted 2-Gaussian and imaged sources agree fairly well with each other. At both energies, those sources exhibit tails extending over 30 fm of relative distance, in the longitudinal z -direction. The failure of the single-Gaussian source to reproduce the correlation moments at low q , observed in Fig. 1, appears to be related to the failure in producing such a tail at large r . A non-Gaussian enhancement in the outward x -direction further develops in the imaged and 2-Gaussian sources between the energies of $\sqrt{s} = 8.9$ A GeV and $\sqrt{s} = 17.3$ A GeV. The sources in Fig. 2 are most compact in the y direction. A tail in the source in the z direction is expected in connection with a strong collective expansion of the system along the beam [6]. Greater extension in the x - than the y -direction and the tail in the x -direction can be associated with emission extended over time. Low transverse momenta have been purposely selected for the analysis

to eliminate any significant effects of Lorentz γ -factors.

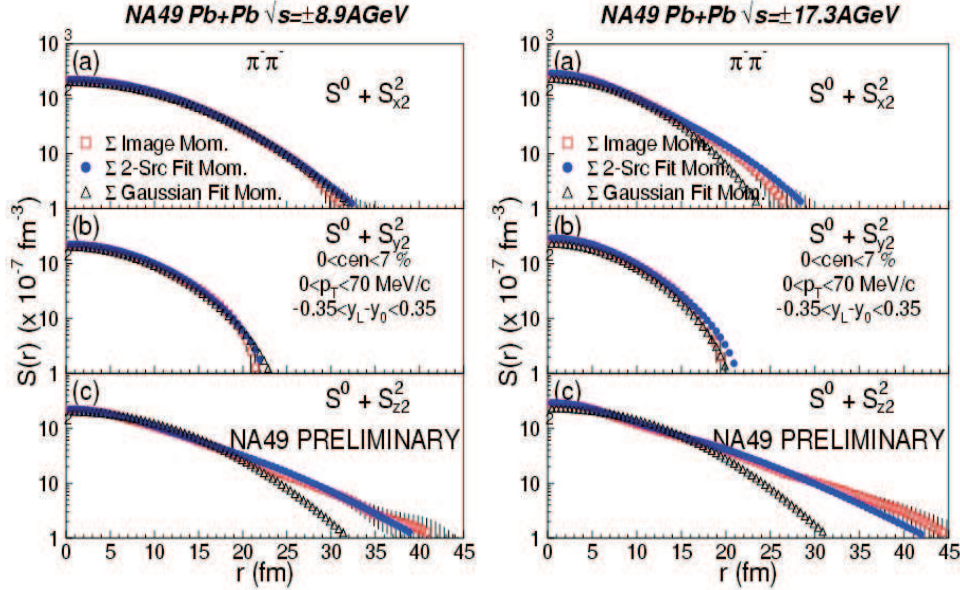


Fig. 2. Relative midrapidity $\pi^- \pi^-$ source in central Pb + Pb collisions along x , y and z coordinate axes, from summing the $\ell \leq 2$ angular components of the source. The left and right panels represent, respectively, source in collisions at $\sqrt{s} = 8.9$ A GeV and $\sqrt{s} = 17.3$ A GeV. Squares represent source values obtained by imaging the angular components of correlation functions measured by the NA49 Collaboration [8]. Triangles represent results of the fit to the measured correlation moments [9] with a source in the form of an anisotropic Gaussian. Circles represent results of the fit to the measured correlation moments with a source combining two anisotropic Gaussians.

Extended non-Gaussian tails in the longitudinal z -direction are further observed in central collisions at RHIC energies. Figure 3 shows the source values extracted from the analysis of $\ell \leq 4$ angular moments of midrapidity correlations measured by the PHENIX Collaboration in central Au + Au collisions at $\sqrt{s} = 200$ A GeV. Again, a fit with a single Gaussian to the correlation functions fails to produce the tail along z -axis emerging from the imaging. The imaged source also exhibits some tail in the outward direction which is not there in the single Gaussian source.

Figure 3 compares further the sources extracted from PHENIX data to those predicted by model calculations. The Therminator model [10], represented in the left panels, has been successful in the past to reproduce Gaussian-source parameters extracted from correlation sources corrected for Coulomb effects. The model supplements short-range features of a source with long-range features due to resonance decays. In the left panels of Fig. 3, it is observed that the model can fully explain

only the experimental source values in the y -direction and partly in the z -direction. However, the model fails completely as far as the long-range features of the imaged source in the x direction. The latter is quite independent of whether the resonance decays take place or are suppressed.

The multi-phase transport model (AMPT) [11] follows the dynamics of both partonic and hadronic phases and includes resonance decays. As is apparent in the right panels of Fig. 3, the model describes fairly well the imaged source features along the x and z directions but fails rather dramatically with respect to the y direction.

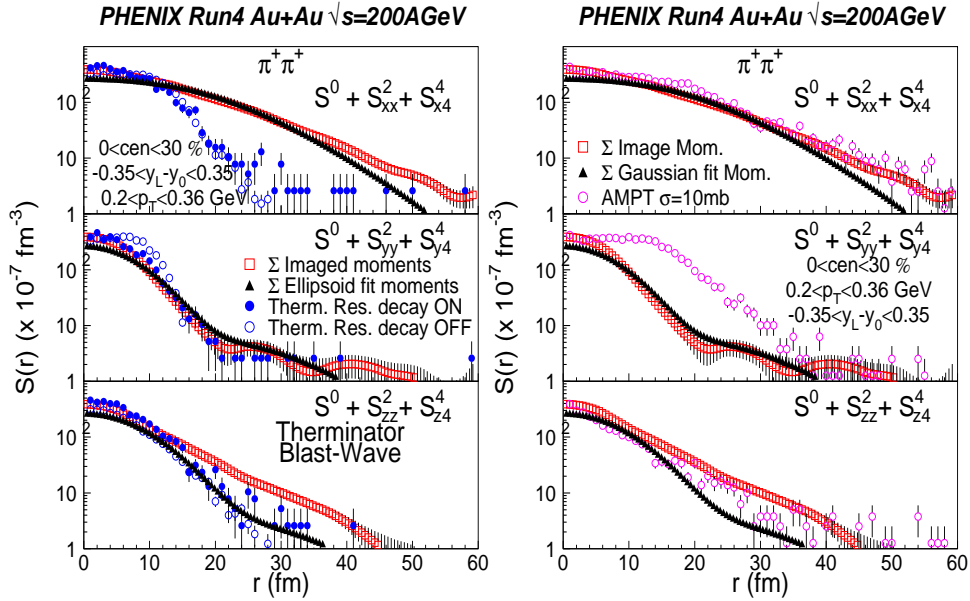


Fig. 3. Relative midrapidity $\pi^+\pi^-$ source in central Au + Au collisions at $\sqrt{s} = 200$ A GeV, along x , y and z coordinate axes, from summing the $\ell \leq 4$ angular components of the source. Squares represent source values obtained by imaging the angular components of correlation functions measured by the PHENIX Collaboration [9]. Triangles represent results of the fit to the measured correlation moments [9] with a source in the form of an anisotropic Gaussian. In the left panels, circles represent a fit using the Therminator model [10, 12] with, respectively, resonance decays operating, for full circles, and switched off, for open circles. In the right panels, circles represent results of the AMPT model [11].

5. Conclusions

As demonstrated with examples of the analyses of NA49 and PHENIX correlation measurements, the expansion in Cartesian harmonics represents a practical strategy

for summarizing correlation functions and for accessing sources shapes. The strategy is capable of producing a wealth of detail on emission sources and challenging this way theoretical interpretations of the data.

Acknowledgments

Results in this paper stem from collaborations with David Brown, Paul Chung and Scott Pratt. This work was supported by the U.S. National Science Foundation under Grants PHY-0245009 and PHY-0555893.

Note

a. E-mail: danielewicz@nscl.msu.edu

References

1. U. A. Wiedemann and U. W. Heinz, *Phys. Rept.* **319** (1999) 145.
2. M. Lisa, S. Pratt, R. Soltz and U. Wiedemann, *Annu. Rev. Nucl. Part. Sci.* **55** (2005) 357.
3. M. Gyulassy and D. Rischke, *Nucl. Phys. A* **608** (1996) 479.
4. D. A. Brown and P. Danielewicz, *Phys. Lett.* **B398** (1997) 252.
5. J. Applequist, *J. Phys. A: Math. Gen.* **22** (1989) 4303.
6. P. Danielewicz and S. Pratt, *Phys. Rev. C* **75** (2007) 034907.
7. D. A. Brown and P. Danielewicz, *Phys. Rev. C* **64** (2001) 014902.
8. P. Chung and P. Danielewicz, in *Proceedings of Workshop on Particle Correlations and Femtoscopy, Sao Paulo, 2006* .
9. P. Chung, P. Danielewicz, W. Holzmann, R. Lacey and J. Alexander, in *Proceedings of Workshop on Particle Correlations and Femtoscopy, Kromeriz, 2005* .
10. A. Kisiel, W. Florkowski, W. Broniowski and J. Pluta, *Phys. Rev. C* **73** (2006) 064902.
11. B. Zhang, C. M. Ko, B.-A. Li and Z.-W. Lin, *Phys. Rev. C* **61** (2000) 067901.
12. A. Kisiel, T. Taluc, W. Broniowski and W. Florkowski, *Computer Physics Communications* **174** (2006) 669.